Computer Fraud and Security
ISSN (online): 1873-7056

The Study on Mesh Optimization and Computational Efficiency Balance in Magnetic Network Modeling of Magnetic-Saturated Controlled Reactor

Mingxing Tian [12*], Yuexin Li [12], Xun Zhu [13], Ying Wang [12]

[1]*School of Automation & Electrical Engineering, Lanzhou Jiaotong University, Lanzhou, China*

[2]*Rail Transit Electrical Automation Engineering Laboratory of Gansu Province, Lanzhou Jiaotong University, Lanzhou, China*

[3] *ETAP Power System Simulation And Analysis Joint Laboratory, Lanzhou Jiaotong University, Lanzhou, China*

**Corresponding author: tianmingxing@mail.lzjtu.cn*

Abstract:

In response to the dynamic reactive power demand surge caused by new energy grid integration, Magnetic-Saturated Controlled Reactor (MSCR) has become an ideal compensation device by virtue of its fast response and continuous regulation capability, but its modelling complexity and computational efficiency need to be solved urgently. This paper takes MSCR as the research object and focuses on the optimisation strategy of mesh dissections for magnetic network models, seeking a balance between computational accuracy and solution efficiency, and verifying the validity of the model through an experimental platform. Firstly, the magnetic leakage effect is considered and the magnetic flux tube equivalence method is adopted to establish the MSCR magnetic network model, and the validity of the model is verified by the measured data. Through the differential grid dissection of the magnetic valve region, it is revealed that the computational efficiency of the magnetic network model is about 100 times higher than that of the finite element method, and the error converges with the grid encryption; under the full-load condition, the local grid encryption of the magnetic valve section can significantly reduce the error, while the sparse mesh error is already very small in the case of no-load, and the optimization method based on the load-grid correlation is further proposed to realize the optimization of no-load and full-load regions by dynamically adjusting the mesh density. By dynamically adjusting the mesh density to achieve sparsification in the no-load region and local encryption in the full-load region, the relative variation of the calculation results under full working conditions is controlled within 1%, which effectively reduces the impact of load fluctuations on the calculation accuracy. This method realizes the dynamic balance between accuracy and efficiency in the modeling of complex electromagnetic devices, and provides theoretical support for the optimization of MSCR function and the engineering promotion of magnetic network model. The research results not only provide theoretical support for the engineering design of MSCR, but also provide important technical support for the system-level simulation of other electromagnetic devices, as well as the real-time simulation and safe and stable operation of smart grid.

Keywords: Magnetic-Saturation Controlled Reactor; Magnetic Network Model; Mesh Division; Error Convergence Characteristics.

INTRODUCTION

With the continuous expansion of modern power systems, reactive power balance and voltage stability have faced severe challenges, placing higher demands on dynamic reactive power compensation [1]. Traditional reactive power compensation devices, such as capacitors and fixed reactors, exhibit inherent limitations in response speed and regulation flexibility, making them insufficient for the needs of modern power grids [2,3]. Meanwhile, the widespread use of power electronic equipment has introduced issues such as harmonic distortion and voltage fluctuations, further deteriorating power quality. As a result, the development of high-efficiency, fast-response reactive compensation devices has become a critical requirement for the optimized operation of power systems.

The magnetically controlled reactor based on magnetic saturation (MSCR), as a new type of reactive power compensation device, has demonstrated significant application value in power systems due to its advantages in rapid voltage regulation, precise reactive power compensation, and suppression of switching overvoltages [4]. It

achieves continuous adjustment of reactance by utilizing the magnetic saturation characteristics of magnetic valves to change the magnetic permeability. However, traditional MSCRs suffer from problems such as low control precision, high losses, slow response, and complex modeling, which severely limit their engineering applications [5–7]. Therefore, establishing an accurate and efficient mathematical model of MSCR to enhance its design optimization is an urgent issue to be addressed.

In the field of electromagnetic device modeling, the finite element method (FEM), based on electromagnetic field theory, is widely applied [8–10], but its large computational burden makes it unsuitable for real-time simulation [11–13]. Conventional approaches often decouple the electromagnetic devices from system-level analysis, neglecting coupling effects and compromising overall system optimization [14–16]. To address these challenges, equivalent magnetic network models based on magnetic circuit concepts have gained wide attention due to their computational efficiency [17,18]. Studies have shown that for calculating leakage magnetic fields in large transformers, magnetic network methods can produce results in seconds, while FEM may require several days. Similarly, in dynamic field-circuit coupling optimization, magnetic network methods exhibit significantly higher computational efficiency than FEM [19].

MSCR modelling requires a balance between equivalent magnetic circuit models and finite element models: the former is computationally efficient but has limited accuracy, while the latter is highly accurate but computationally expensive [20,21]. The magnetic network model combines the advantages of both, but its accuracy is affected by factors such as leakage flux, core stack structure, and mesh dissections. In this study, the following key issues are addressed: (1) under the premise of considering the leakage flux effect, the sparse dissections in the main region of the core and the local encryption in the high-gradient region of the magnetic valves are achieved through the differentiated mesh dissecting strategy, which significantly improves the computational efficiency while guaranteeing the accuracy; (2) the flux-tube-equivalent method is adopted to establish the magnetic network model, which provides a method for the model building and solving; (3) the effect of the number of mesh dissections on the error is nonlinear with the change of load condition, and the optimization method of load-grid correlation is further proposed to provide a new idea for the optimization of the magnetic network modeling; (4) By adopting the optimization method of load-grid correlation, the relative change of the error of the calculation results under the full working condition is controlled within 1%, which effectively reduces the influence of load fluctuation on the calculation accuracy.

This study establishes a magnetic network model for MSCR, achieving a favorable balance between computational accuracy and efficiency, and providing theoretical support for its optimal design. The results not only apply to system-level simulations of other electromagnetic devices such as transformers and motors but also offer critical technical support for real-time simulation and secure, stable operation of smart grids.

MODELING PARAMETERS OF MSCR

Taking the parameters of a physical MSCR prototype as an example, the core material is 30Q130 silicon steel sheet, and the geometric structure parameters of the prototype are shown in Table 1. The magnetic valve adopts a single-valve structure, and the core thickness is 6.5 cm. The large cross-sectional area of the core is three times that of the magnetic valve.

Table 1 Rated Parameters of the MSCR Experimental Prototype

Parameter	Numerical value	Parameter	Numerical value
Quantitative	2.2 kVar	Cross-sectional area of iron core	0.0042 m^2
Rated voltage	220 V	Magnetic valve length	0.01 m
Core width	0.065 m	Magnetic valve cross-sectional area	0.0014 m^2
Core length	0.065 m	Height of AC and DC windings	0.07 m
Core section width	0.18 m	AC and DC winding turns	400

MESH GENERATION OF THE MSCR

According to the principle of minimum magnetic flux path and the magnetic field distribution characteristics of the MSCR, the left and right yokes, upper and lower yoke core columns, and the magnetic valve region are divided into different mesh elements. Due to significant magnetic leakage in the magnetic valve area, the air gap near the magnetic valve and core columns is also meshed separately from other regions. The initial mesh division of the MSCR is shown in Figure 1.

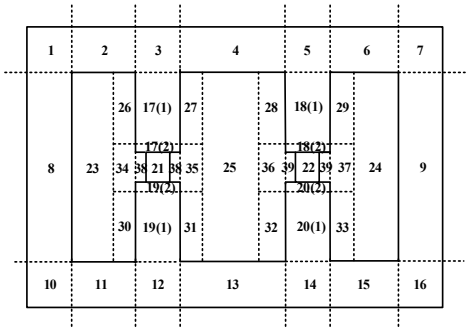

Figure 1. Preliminary Grid Partition Diagram of MSCR

The valve segment is the region where the magnetic flux changes most drastically within the iron core, and it has a significant impact on the magnetic field distribution[22]. Therefore, performing fine mesh division in this area helps improve the accuracy of the simulation results and avoids errors caused by insufficient mesh resolution. Due to the influence of edge effects, the magnetic flu corner regions of the MSCR valve segment is significantly higher than in other areas. Taking the left valve segment as an example, it is subdivided into the following two types of mesh division, as shown in Figures 2 and 3.

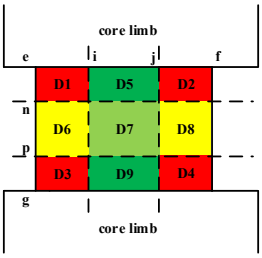

Figure 2. Schematic Diagram of the First Refined Mesh at the Magnetic Valve

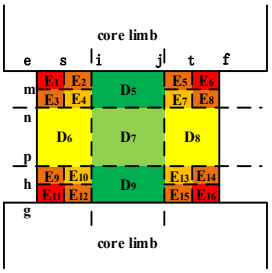

Figure 3. Schematic Diagram of the Second Refined Mesh at the Magnetic Valve

MAGNETIC FLUX TUBE EQUIVALENT METHOD

Using the magnetic flux tube equivalence method, the MSCR is modeled with magnetic flux tube mesh elements as shown in Figure 4. The center of each mesh element is connected to four magnetic reluctances (R1x, R2x, R1y, R2y) in the transverse and longitudinal directions. The length, width, and height of the mesh element are represented by lx, lw, and ly, respectively. The magnetic permeability calculation formula is as follows:

$$\begin{cases} R_{1x} = R_{2x} = \dfrac{l_x / 2}{\mu S_x} \\ R_{3y} = R_{4y} = \dfrac{l_y / 2}{\mu S_y} \end{cases} \quad (1)$$

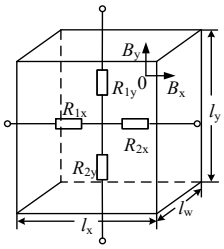

Figure 4. Schematic Diagram of a Magnetic Flux Tube Element

EQUIVALENT MAGNETIC FLUX TUBE MODEL OF MSCR

Based on the grid division in Figure 1, the magnetic network model of the MSCR is established using the magnetic flux tube equivalent method. The model for the left half is shown in Figure 5, and the model for the right half is symmetric to the left half along the longitudinal central axis. FAC1 and FAC2 represent the magnetomotive forces of the AC windings on the iron core columns, while FDC1 and FDC2 represent the MMFs of the DC control windings on the iron core columns.

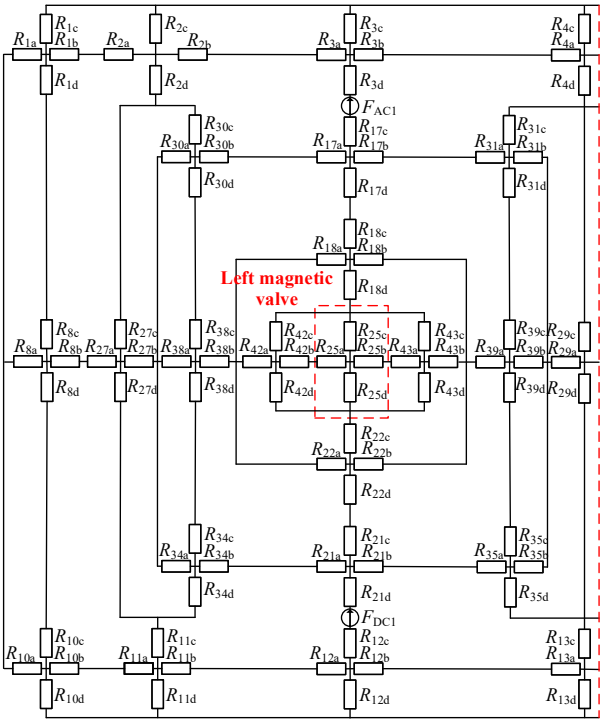

Figure 5. First Equivalent Magnetic Network Model of the MSCR

Taking the left magnetic valve segment as an example, the equivalent magnetic network models corresponding to Figures 2 and 3 are shown in Figures 6 and 7, respectively. By substituting Figures 6 and 7 into the red region of Figure 5, while keeping the remaining parts unchanged, new magnetic network models are established.

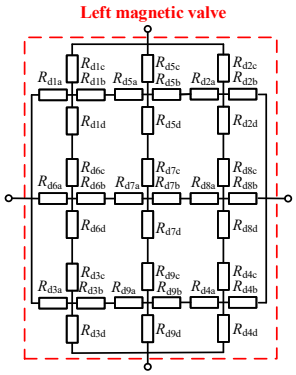

Figure 6. Equivalent Magnetic Network Model of the First Type of MSCR Magnetic Valve Section

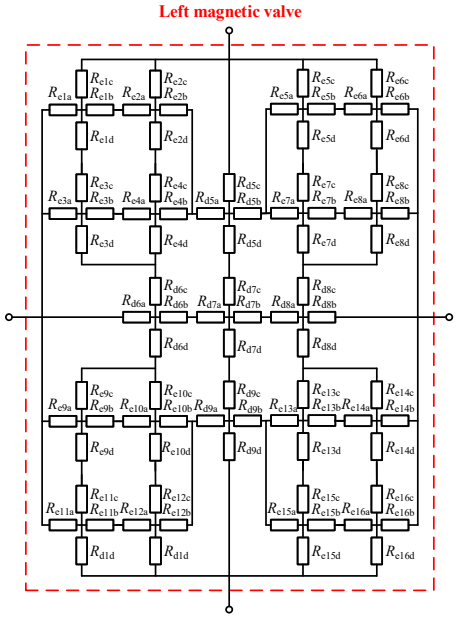

Figure 7. Equivalent Magnetic Network Model of the Second Type of MSCR Magnetic Valve Section

CALCULATION OF THE MSCR MAGNETIC NETWORK MODEL

In the magnetic network modeling of a MSCR, the AC and DC excitation magnetomotive forces are the fundamental basis for constructing the nodal equations[23]. The DC excitation winding and the AC working winding act together on the magnetic circuit of the core. Their MMFs can be defined separately as follows:

$$\begin{cases} F_{\mathrm{AC}}(t) = N_{\mathrm{AC}} i_{\mathrm{AC}}(t) \\ F_{\mathrm{DC}} = N_{\mathrm{DC}} I_{\mathrm{DC}} \end{cases} \qquad (2)$$

The magnetic reluctance of any segment of the core in the main magnetic circuit is calculated as:

$$R_{\mathrm{m}i} = \frac{l_i}{\mu_i S_i} \qquad (3)$$

where l_i, S_i, and μ_i represent the length, cross-sectional area, and magnetic permeability of the i-th segment of the core, respectively.

The commonly used ferromagnetic material in MSCR, 30Q130, is characterized by low loss and high magnetic permeability[24]. Its critical saturation magnetic field intensity Hs is 270 A/m, and the critical saturation magnetic flux density Bs is 1.8 T. In this study, a piecewise function magnetization model is used for simulation analysis, as shown in Equation (4).

$$B=\begin{cases}\mu_1 H, & -H_s \le H \le H_s \\ \mu_0\left(H-H_s\right)+B_s, & H>H_s \\ \mu_0\left(H+H_s\right)-B_s, & H<-H_s\end{cases} \quad (4)$$

Let l_g and S_g represent the air gap length and cross-sectional area, respectively, and μ_0 be the permeability of free space. The magnetic reluctance at the air gap is calculated as:

$$R_q=\frac{l_g}{\mu_0 S_g} \quad (5)$$

Based on the analogy between magnetic circuits and electrical circuits, the nodal magnetic potential method is used to solve the equivalent magnetic network. The nodal magnetic potential equation is given by:

$$G\varphi=\phi \quad (6)$$

where G is the magnetic conductance matrix; φ is the vector of nodal magnetic potentials; ϕ is the external magnetic flux source vector.

By solving the nodal magnetic potential equation, the magnetic fluxes in each branch of the MSCR magnetic circuit and the nodal magnetic potentials can be obtained. Based on the calculated nodal magnetic potentials, the MMF of each branch can be determined, from which the mathematical expression of the working current of the MSCR can be derived:

$$i_k=\frac{F_k}{N}=\frac{\phi_k R_k}{N} \quad (7)$$

where ϕ_k and R_k are the magnetic flux and reluctance of the k-th segment of the core, respectively.

COMPARATIVE ANALYSIS OF THE OPERATIONAL CHARACTERISTICS BETWEEN THE MSCR MAGNETIC NETWORK AND FINITE ELEMENT MODELS

The working current from the 3D finite element model is used as the reference for comparative analysis. The constructed model is shown in Figure 8.

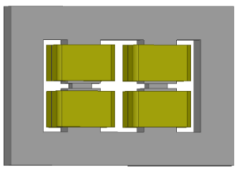

Figure 8. 3D Finite Element Model

The simulation time for the magnetic circuit network model is from 0 to 1 second. Since the focus of the study is on steady-state accuracy, only the steady-state waveforms from 0.94 to 1 second are extracted for comparison. The comparison of the three magnetic circuit network models with the reference values is illustrated in Figure 9. The relative error in the working current calculation and the response speed comparison are presented in Table 2.

Table 2 Comparison of Computational Efficiency between MSCR Magnetic Network Model and Finite Element Model

Operating condition	Computational target	Peak current (A)	Relative error (%)
No-Load	MSCR Magnetic Network Model 1	0.2872	0.985
	MSCR Magnetic Network Model 2	0.2864	0.703
	MSCR Magnetic Network Model 3	0.2861	0.598
	MSCR Finite Element Model	0.2844	/

Half-Load	MSCR Magnetic Network Model 1	9.3798	4.80
	MSCR Magnetic Network Model 2	9.2187	3.00
	MSCR Magnetic Network Model 3	9.1382	2.10
	MSCR Finite Element Model	8.9502	/
Full-Load	MSCR Magnetic Network Model 1	15.9467	12.15
	MSCR Magnetic Network Model 2	15.2557	7.29
	MSCR Magnetic Network Model 3	14.8590	4.50
	MSCR Finite Element Model	14.2191	/

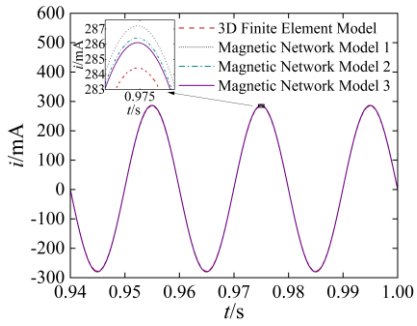

(a) No-load

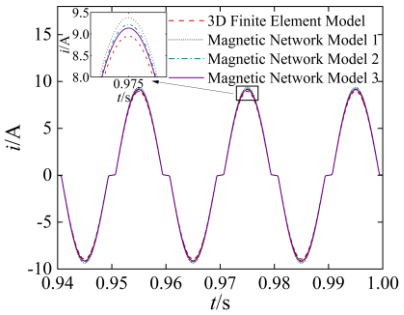

(b) Half-load

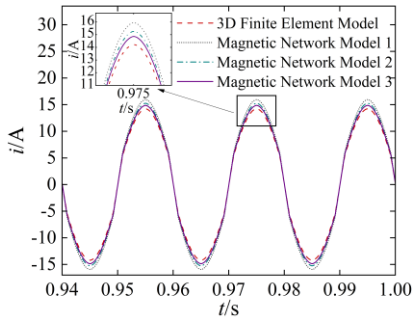

(c) Full-load

Figure 9. Comparison of Working Currents in Different MSCR Models

By calculating the error decrease of the magnetic network model, it can quantitatively reveal the magnitude of the improvement of the magnetic field calculation accuracy by adjusting the density of grid profiles at the magnetic valve section. From the magnetic network model I to model III, the number of grids is gradually increased, and it can be observed that increasing the number of grid sections at the magnetic valve affects the error in the following pattern:

(1) The overall trend of the number of grids and error reduction: the error reduction is non-linearly convergent with the number of grids. When the number of grids is initially increased, the error is significantly reduced; however, as the grids are further encrypted and when a certain density is reached, the error improvement gradually slows down, showing a diminishing returns effect. This is due to the dominance of the discretisation error under coarse grid dissection, such as the local truncation error due to excessive magnetic field gradient; whereas the discretisation error tends to be close to zero when the fine grid approaches the continuous solution, but the computational cost rises exponentially. The error is usually related to a power of the mesh size *h*:

$$\text{errors} \propto h^{p} \qquad (8)$$

where p is the convergence order (e.g., linear cells , but nonlinear materials may reduce the actual convergence rate).

(2) The error decreasing amplitude shows significant load-dependent characteristics, with the largest error decreasing amplitude under full-load condition, followed by half-load condition, and the smallest error decreasing amplitude under no-load condition. The intrinsic mechanism lies in the following: when the MSCR is in full load condition, the gradient of magnetic field rises sharply due to the deep magnetic saturation of the magnetic valve segment, and the strong nonlinear effect makes it difficult to accurately characterize the local magnetic field mutation in the traditional homogeneous mesh, while the optimized non-uniform mesh effectively improves the resolving ability of the local permeability mutation by encrypting the high-gradient area cells, thus significantly reducing the discretization error; in half-load condition, the valve is partially saturated, and the distribution of magnetic field is partially saturated, and the error reduction is the smallest in no-load condition. Under the half-load condition, the magnetic valve is in a partially saturated state, and the complexity of the magnetic field distribution is between the full-load and no-load conditions, at which time the correction effect of the grid optimisation on the error is weakened synchronously; in the case of no-load condition, the magnetic valve segment has not entered the saturation zone, the uniformity of the magnetic field distribution is high, and the discretisation error is at a relatively low level, so that the marginal benefit of the grid refinement is the most limited.

Based on the above quantitative analysis of the error pattern and load characteristics, the correlation model between the number of grids and the computational error can be established, and the load-dependent characteristics can be clarified. Based on this, a grid optimization strategy is proposed: under no-load condition, due to the uniform magnetic field distribution and low error sensitivity, the sparse grid configuration can save computational resources; under half-load condition, the magnetic valve segment is partially saturated, and the medium density grid can ensure the computational accuracy while achieving the optimization of the computational efficiency; under full-load condition, the deep saturated region of the magnetic valve segment is encrypted by a local grid, and the high gradient zone with significant nonlinear effect is preferred to increase the grid density, so that the computational error can be optimized. Under full load condition, local grid encryption is implemented for the deep saturated area of the magnetic valve segment, and the grid density is increased in the high gradient area with significant nonlinear effect, so that the computational error can be controlled within 5%, while avoiding the waste of computational resources caused by overall encryption. This load-grid correlation optimisation method effectively balances the calculation accuracy and efficiency, and provides a practical optimisation scheme for engineering applications.

However, the computation time increases with the number of mesh elements. Taking Magnetic Network Model 3 as an example, a further analysis of the response speed between the magnetic network model and the finite element method is shown in Table 3.

Table 3 Comparison of Computational Efficiency between MSCR Magnetic Network Model and Finite Element Model

Operating condition	Computational target	Response speed (t_1/s)
No-load	MSCR Magnetic Network Model	203.323
	MSCR Finite Element Model	21288.0
Half-load	MSCR Magnetic Network Model	218.489
	MSCR Finite Element Model	21186.0
Full-load	MSCR Magnetic Network Model	198.593
	MSCR Finite Element Model	20296.0

From Table 3, it can be found that although the finely dissected mesh can improve the computational accuracy of the magnetic network model, its computational efficiency is still significantly better than that of the finite element method. Even if the finest mesh dissection scheme is used at the magnetic valves, the computational speed of the magnetic network model is still significantly faster than that of the finite element simulation, indicating that the magnetic network method has high computational efficiency while guaranteeing the accuracy, and is suitable for application scenarios of optimised design and real-time control of large-scale power equipment that require fast solutions.

COMPARISON OF THE SIMULATION OF THE IMPROVED MAGNETIC FIELD CHARACTERISTICS

The magnetic network model, as an efficient computational method, can not only calculate the operating characteristics of MSCR, but also effectively simulate the dynamic changes of magnetic field characteristics. In this study, a load-grid correlation optimisation method is proposed to systematically improve the traditional magnetic network model based on the results of simulation and comparison of operating characteristics. A differentiated mesh splitting strategy is adopted to meet the computational accuracy requirements under different load conditions: under unloaded conditions, the sparsely split magnetic network model I is used as the base model for comparison with the finite element; under half-loaded conditions, the moderately split magnetic network model II is used for comparison; and for the full-loaded conditions, where the computational error is more significant, the magnetic network model III is used for comparison to improve the computational accuracy of the model. For the full-load condition, the magnetic network model III constructed by the fine-dissection processing is used for comparison in order to improve the calculation accuracy. Taking the change of magnetic flux density at the MSCR magnetic valve as an example, the specific simulation results are shown in Fig. 10.

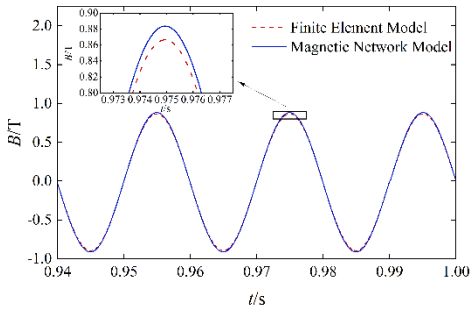

(a) No-load

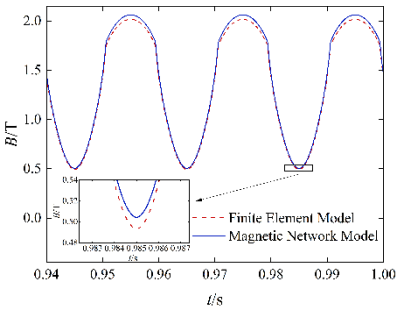

(b) Half-load

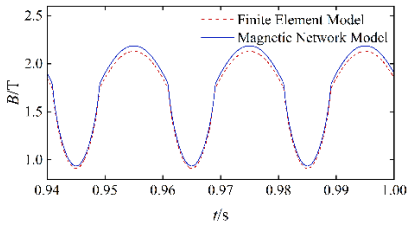

(c) Full-load

Fig. 10 Comparison of the change in magnetic flux density between the improved magnetic network model and the finite element model

In order to further quantify the accuracy of the analytical model, this study takes the finite element calculation results as the benchmark and selects the peak flux density as the comparison parameter, and the error comparison data under different loading conditions are detailed in Table 4.

Table 4 Comparison of magnetic flux density between MSCR magnetic network model and finite element model

Operating condition	Computational target	Peak magnetic flux density (Bm/T)	Calculated relative error (%)
No-load	MSCR Magnetic Network Model	0.8836	1.97
	MSCR Finite Element Model	0.8665	/
Half-load	MSCR Magnetic Network Model	2.0609	2.25
	MSCR Finite Element Model	2.0155	/
Full-load	MSCR Magnetic Network Model	2.1875	2.70
	MSCR Finite Element Model	2.1300	/

The simulation results show that the improved magnetic network model is in good agreement with the finite element model in terms of the flux density variation characteristics. Comparative analysis shows that the relative change in the error of the improved magnetic network model from no-load to full-load conditions does not exceed 1%, which verifies that the optimisation scheme can significantly reduce the sensitivity of load fluctuation to the

calculation accuracy. The magnetic network model constructed based on the load-mesh correlation optimisation method significantly improves the simulation accuracy while maintaining the computational efficiency, which achieves an optimal balance between computational efficiency and accuracy. This result not only verifies the feasibility of the proposed optimization method, but also fully proves the effectiveness of the method in improving the computational performance of the magnetic network model, which provides a reliable modelling method for the characterization of electromagnetic devices under complex working conditions.

VALIDATION OF THE MSCR MAGNETIC NETWORK MODEL AGAINST EXPERIMENTAL PROTOTYPES

In this paper, the MSCR experimental prototype is used to verify the accuracy of the established magnetic network model of magnetic saturated controllable reactor. The equipment used for the experiment includes the MSCR prototype, voltage regulator, oscilloscope, dc power supply, voltage and current measurement equipment and dc power supply trigger board. In this paper, the he-excited magnetically saturated controllable reactor (MSCR) is selected as the experimental object to carry out the validation work. The physical diagram of the prototype is shown in Fig. 11, and the specific parameters are listed in Table 1.

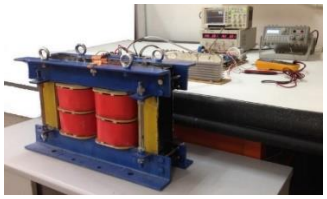

Fig. 11 MSCR experimental prototype

In the test, the MSCR prototype is supplied with 220V power at industrial frequency by a voltage regulator, and the DC bias current and output capacity are changed by adjusting the thyristor trigger angle of the control winding from 0° to 180°. Considering the high gradient characteristics of the magnetic field in the magnetic saturation region, the experimental verification is mainly carried out under load conditions. Under the premise of ensuring that all the measurement lines are connected correctly and the instrument parameters are set reasonably, the waveforms of the operating currents under load conditions are measured and compared with the simulation results, as shown in Figs. 12 and 13.

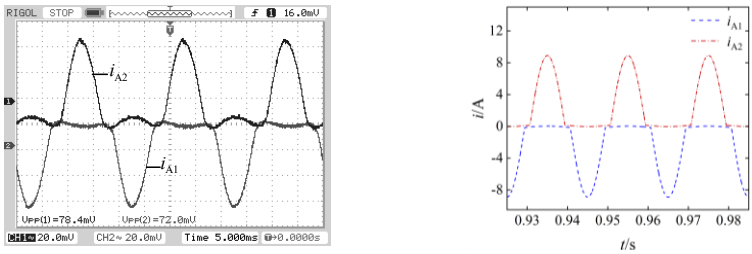

(a) Measured waveforms (2A/div) (b) Simulated waveforms

Fig. 12 The current in the two-branch circuit of the MSCR when the triggering angle is $\alpha = 111°$

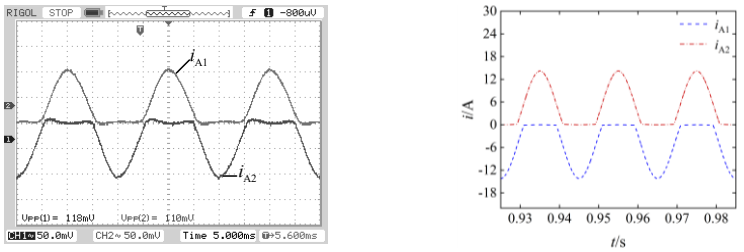

(a) Measured waveform (5A/div) (b) Simulated waveform

Fig. 13 The current in the two-branch circuit of the MSCR when the triggering angle is $\alpha = 80°$

By observing the current waveform characteristics in Figs. 12 and 13 under different DC bias, it can be found that

the aberration degree of the operating current waveform shows an obvious weakening trend with the gradual increase of the bias voltage of the control winding, and this phenomenon is closely related to the fact that the working point tends to be linearised after the magnetisation state of the core enters into the deep saturation region. Comparing the measured data and simulation results of the physical prototype, it can be found that there is a high degree of consistency in waveform characteristics, amplitude change and phase relationship, which confirms the validity of the magnetic network model constructed in this paper in different operating conditions, and provides a solid theoretical basis for subsequent engineering applications.

CONCLUSION

In this paper, the balance between mesh optimisation and computational efficiency in MSCR magnetic network modelling is investigated, a magnetic network model considering the leakage effect is established, and differential mesh dissections of the magnetic valve region are performed, revealing that with the increase of the number of grid cells in the magnetic valve segment of the MSCR, the operating currents computed by the magnetic network model are gradually close to the finite-element results and the errors show a tendency to converge. Compared with the finite element method, the computational efficiency is improved by about 100 times. By quantitatively analysing the relationship between mesh density and computational error, the optimisation rules of sparse meshing under no-load condition and locally refined meshing under full-load condition are clarified, and the proposed load-grid correlation optimisation method effectively balances the computational accuracy and efficiency. Comparison of the magnetic field characteristics between the load-grid correlation optimisation model and the finite element model is carried out, and the comparison results show that the relative change of the calculation results from no-load to full-load conditions is no more than 1%, which verifies that the optimisation scheme can significantly reduce the sensitivity of load fluctuation to the calculation accuracy. Finally, the experimental platform of MSCR prototype was built to test the operating characteristics under load conditions, and the high degree of consistency between experiment and simulation fully proves the effectiveness of the established MSCR magnetic network model. The research results in this paper provide a theoretical basis for the digital design and optimisation of MSCR, and at the same time lay a methodological foundation for the popularisation and application of magnetic network models in complex electromagnetic devices. Future research can be combined with multidisciplinary cross technology to further improve the comprehensive performance and engineering applicability of the model.

FUNDING

This work supported by National Natural Science Foundation of China (52167013), Key Program of Natural Science Foundation of Gansu Province (22JR5RA320) and Natural Science Foundation of Gansu Province (24JRRA244).

REFRENCES

[1] Yu B, Wang D . Application of magnetically controlled reactor-type static reactive power compensation device[J]. Shanghai Electric Technology, 2020, 13(02): 16-19+56.

[2] Ding H. Discussion on reactive power compensation technology in automation control system[J]. China Equipment Engineering, 2025, (05): 103-105.

[3] Zhan X, Wang J, Guo G, et al. Coordinated control strategy of reactive power compensation based on a flexible distribution network transformer[J]. Frontiers in Energy Research, 2024, 12.

[4] Wang Q P, Bai B D, Chen D Z, et al. Dynamic characterisation and harmonic suppression of 800kV ultra-high voltage magnetically saturated controllable reactor[J]. Journal of Electrotechnology, 2020, 35(S1): 235-242.

[5] Chen Z M, Liu H, Zhong W C, et al. Operating condition assessment model of series reactor-type high impedance transformer[J]. Electronic Design Engineering, 2025, 33(01): 91-95.

[6] Wang G, He J S, Min Y Z, et al. Cut-off frequency improved cooperative denoising method for CEEMDAN-SVD high-voltage shunt reactor acoustic signals[J/OL]. Journal of Electrical Machines and Control, 1-13[2025-04-03].

[7] Guo J Y, Li X P, Zhao J Y, et al. Robust optimisation of reactor core damping based on the uncertainty of air gap structure parameters[J/OL]. Journal of Electrotechnology, 1-13[2025-04-03].

[8] Xie Y, Geng G X, Cai W, et al. Optimised design of permanent magnet synchronous motor with spacer hole rotor structure for efficiency and vibration noise[J/OL]. Chinese Journal of Electrical Engineering, 1-11[2025-04-03].

[9] Zhang K J, Wang B, Wang Y K, et al. Semi-analytical calculation method of permanent magnet motor based on harmonic analysis[J]. Large Motor Technology, 2025, (02): 96-104.

[10] Li H X, Wang D P. Design and structural analysis of high-speed magnetic levitation motor for blower[J]. Microtome, 2025, 53(02): 14-19.

[11] Gao S G, Meng L M, Zhang Y K, et al. Vibration fatigue analysis and defect diagnosis of high-voltage shunt reactor[J]. High Voltage Electrical Apparatus, 2025, 61(01): 215-222.

[12] Yang X X, Wang C Z, Zhang F, et al. A time-stepping finite element model of synchronous motor taking into account the excitation system[J]. Large Motor Technology, 2023, (01): 21-29+36.

[13] Guo X Q, Hua W, Cheng M. Semi-analytical saturated air-gap magnetic field model of switched reluctance motor based on magnetic field modulation theory[J/OL]. Journal of Southeast University (Natural Science Edition), 1-12[2025-04-04].

[14] Yang M, Huang L Y, Sun J H, et al. A review of electromagnetic transient modelling techniques for transformers[J]. High Voltage Technology, 2025, 51(01): 1-20.

[15] Xiong B, Cui G, Bao B Y, et al. Temperature distribution characteristics of permanent magnets in high power density permanent magnet motors based on magneto-thermal coupling method and experimental study[J]. Journal of Electrical Machines and Control, 2024, 28(11): 104-116.

[16] Yang Y, Xu Q W, Miao Y R, et al. Dynamic equivalent magnetic network modelling and multi-field coupling calculation method for magnetic lifting CRDM[J/OL]. Journal of Electrotechnology, 1-14[2025-04-04].

[17] Wu S G, Pang X W, Tong W M, et al. Modelling and analysis of magnetic network of modular stator hybrid excitation synchronous motor[J]. Journal of Electrical Machines and Control, 2023, 27(12): 95-104.

[18] Wang T G, Tian M X, Zhang H Y, et al. Study on the unity of electromagnetic characteristics of controllable reactor based on transformer model[J]. Power Grid Technology, 2023, 47(07): 2947-2956.

[19] Zhang W J, Xu Y L, Tian X, et al. Dynamic equivalent magnetic network model and drive system of permanent magnet synchronous motor with double V-shaped magnet structure[J]. Mechatronics, 2023, 96.

[20] Li W, Cui J N, Zou L M, et al. Optimised design of single magnetic circuit for electromagnetic force generator based on equivalent magnetic circuit method[J]. Vibration and Shock, 2023, 42(12): 309-316.

[21] Christian K, Andreas K, Wolfgang K. Modeling of a permanent magnet linear synchronous motor using magnetic equivalent circuits[J]. Mechatronics, 2021, 76.

[22] Kang M S, & Cho Y H. Loss Reduction in gapped-core-type shunt reactors via magnetic flux distribution improvement[J]. Journal of Electrical Engineering & Technology, 2024, 19, 4445–4453.

[23] Fuchs G, Kugi A, Kemmetmüller W. Magnetic equivalent circuit modeling of a permanent magnet linear synchronous motor composed of curved segments[J]. Mechatronics, 2024, 104103256-103256.

[24] Krämer C, Kugi A, Kemmetmüller W. Optimal force control of a permanent magnet linear synchronous motor based on a magnetic equivalent circuit model[J]. Control Engineering Practice, 2022, 118: 104456.